Quantum-well states with image state character for Pb overlayers on Cu(111)

A. Zugarramurdi,[1,2,3] N. Zabala,[2,3,4] V. M. Silkin,[3,4,5,6] E. V. Chulkov,[3,4,6] and A. G. Borisov[1]

[1]*Institut des Sciences Moléculaires d'Orsay, ISMO, Unité de Recherches CNRS-Université Paris-Sud UMR 8214, Bâtiment 351, Université Paris-Sud, F-91405 Orsay Cedex, France*

[2]*Elektrizatea eta Elektronika Saila, Zientzia eta Teknologia Fakultatea, UPV/EHU, 644 P.K., 48080 Bilbao, Spain*

[3]*Centro de Física de Materiales CFM - Materials Physics Center MPC, Centro Mixto CSIC-UPV/EHU, 20018 San Sebastián/Donostia, Spain*

[4]*Donostia International Physics Center (DIPC), P. de Manuel Lardizabal 4, 20018 San Sebastián/Donostia, Spain*

[5]*IKERBASQUE, Basque Foundation for Science, 48011 Bilbao, Spain*

[6]*Departamento de Física de Materiales, Facultad de Ciencias Químicas, Universidad del País Vasco UPV/EHU, Apto. 1072, 20080 San Sebastián/Donostia, Spain*

(Received 25 May 2012; published 14 August 2012)

We study theoretically the quantum well states (QWSs) localized in Pb overlayers on Cu(111) surface. Particular emphasis is given to the states with energies close to the vacuum level. Inclusion of the long-range image potential tail into the model potential description of the system allows us to show the effect of hybridization between QWSs and image potential states (ISs). The particle-in-a-box energy sequence characteristic for QWSs evolves into the Rydberg series converging towards the vacuum level. The electron density of the corresponding states is partially moved from inside the metal overlayer into the vacuum. The decay rates due to the inelastic electron-electron scattering decrease with increasing energy, opposite to "conventional" QWSs and similar to the ISs. Many-body and wave packet propagation calculations of the inelastic decay rates are supplemented by simple analysis based on the phase accumulation model and wave-function penetration approximation. This allows an analytical description of the dependence of the QWS/ISs hybridization on different parameters and, in particular, on the overlayer thickness.

DOI: 10.1103/PhysRevB.86.075434 PACS number(s): 73.21.Fg, 73.20.At, 73.50.Gr

I. INTRODUCTION

For metal films deposited on different substrates, potential barriers at the film/vacuum and film/substrate interface confine electrons in the direction perpendicular to the surface of the film. If the thickness of the film is smaller than the electron mean free path, the bulk electronic structure of the film material evolves into a set of subbands characterized by the quantized electron motion perpendicular to the film, and bulklike dispersion in the film plane.[1–10] Depending on the reflectivity of the film/substrate interface, the quantized electronic states can be either stationary in one-electron picture or decaying into the electronic states of the substrate, via resonant electron transfer.[6] One then uses the terms quantum well states (QWSs)[1–6] or quantum well resonances (QWRs),[7–11] respectively. The QWSs can be readily understood in terms of the discrete level structure of a one-dimensional (1D) potential well. In particular, the semiclassical description based on the phase accumulation model[12,13] appears extremely efficient in describing the energies of the QWSs at $\bar{\Gamma}$ point.[4–6] The semiclassical description of the QWRs can be performed with a Fabry-Perot-type approach.[4,6–8,10] As a consequence of the quantization of the electronic structure, many properties of metal films show a quantum size effect,[3–6,14,15] i.e., a (oscillatory) dependence on the film thickness D, where D can be changed only by the discrete amount given by the interlayer spacing a. Because of the fundamental and practical interest quantum size effects have been studied in detail for the work function and surface energy,[16–20] chemical reactivity,[21] magnetic coupling,[5,22–24] Rashba effect,[25,26] etc.

Development of the scanning tunneling spectroscopy (STS) and time-resolved two-photon photoemission techniques (TR-2PPE) has recently placed the topic of excited electron dynamics in thin metallic films in a focus of thorough research. Indeed, the lifetime of excited electronic states is a key quantity in surface science directly controlling the efficiency of many chemical and photochemical processes.[27,28] The lifetime sets the duration of the excitation and, when combined with the group velocity, it also determines the spatial range of the excitation. For metals and metallic nanostructures at surfaces, several decay channels determine the dynamics of excited electrons for which the total decay rate Γ (proportional to the inverse of the lifetime τ) can be expressed as a sum of different contributions:[29,30]

$$\Gamma = \hbar/\tau = \gamma_{1e} + \gamma_{e\text{-}e} + \gamma_{e\text{-ph}} + \gamma_{\text{def}}. \quad (1)$$

The last term γ_{def} stands for the rate of the decay via defect scattering. The resonant one-electron decay into the substrate is given by the rate γ_{1e}. It is operative for QWRs and depends on the reflectivity of the film/substrate interface as well as on the overlayer thickness. This can be described quantitatively considering an overlayer as a Fabry-Perot resonator.[4,6–8,10] The decay rate due to electron-phonon scattering $\gamma_{e\text{-ph}}$ is relatively small at low temperatures and shows a quantum size effect with the overlayer thickness.[31–35] When the resonant electron transfer into the substrate is impossible, such as for the substrate with projected band gap, the decay via inelastic electron-electron scattering, $\gamma_{e\text{-}e}$, is usually assumed to be the main decay channel at low temperatures and high excitation energies. Particularly detailed experimental and theoretical studies of this deexcitation mechanism have been reported for Pb quantum wells. The TR-2PPE technique has been used for supported Pb films,[36–39] and STS experiments have been performed on large well characterized Pb adislands.[14,35,40–44] Irrespective of the overlayer thickness, a Fermi liquid type

parabolic dependence of the decay rate on the energy of the QWSs has been found with absolute values close to those obtained in *ab initio* and model calculations[35,45,46] for bulk Pb.

Interpreted as due to the efficient bulklike screening already for relatively thin films,[38] the above finding concerns the QWSs well localized inside the Pb overlayer. At the same time one would expect that, for the energies close to the vacuum level, the QWSs will hybridize with image potential states (ISs) as shown in Ref. 47. The ISs correspond to an excited electron bound in front of the metal surface by the image charge potential. When electron penetration into the metal is prohibited by the projected band gap, ISs form a Rydberg series converging toward the vacuum level E_V with energies at $\bar{\Gamma}$ given by[12,13,48–51]

$$E_V - E_n = \frac{1}{32(n+\alpha)^2}. \tag{2}$$

(Atomic units are used throughout the paper unless otherwise stated). In Eq. (2), $n = 1,2,\ldots$ is the principal quantum number and α is the quantum defect. The electron motion parallel to the surface is quasifree with effective mass close to one.[48,51] The higher is n, the further from the surface is located the excited electron, and the smaller is its coupling with metal bulk electrons so that the lifetime of the image states increases as n^3.[12,29,50–54] The hybridization between QWSs and ISs would alter the weight of the QWS wave function inside the metal film, shifting part of the electron density into the vacuum. Consequently, the energies of the states will change, as well as the many-body decay rates. This has been experimentally confirmed in TR-2PPE studies of the ISs at surfaces of rare-gas adlayers on metal surfaces.[50,51,55–60] In these systems, strong quantum size effects on the lifetimes of the ISs have been found and successfully interpreted as due to the hybridization between the ISs and the QWSs localized in the conduction band of the dielectric adlayer.

The purpose of the present contribution is to show how the QWSs in metallic Pb overlayers on Cu(111) surfaces are modified close to the vacuum level by the hybridization with the ISs. In an earlier paper, we have presented many-body GW calculations of the electron-electron inelastic decay rates for QWSs with energies up to 3 eV with respect to the Fermi level.[45] Here we take a step further and include the classical image potential in the model description of the Pb/Cu(111) system. This allows a detailed study of the effect of QWS/IS hybridization on the energies and decay rates of the excited electronic states in thin metallic overlayers and of the role played by the overlayer thickness.

The paper is organized as follows. In Sec. II, we discuss the theoretical model used for the representation of the Pb/Cu(111) system and methods used for calculations of the many-body $\gamma_{e\text{-}e}$ decay rates. Section III is devoted to the results and their discussion. Finally, in Sec. IV, we give a summary of the work and conclusions.

II. METHODS

A. Model potential

We describe the Pb/Cu(111) system with a model one-electron potential. It is constructed by adding a long-range image potential tail to the effective potential V_{eff} obtained from the self-consistent density functional theory (DFT) calculations within the local density approximation (LDA). The DFT-LDA calculations have been shown to reproduce fairly well the most stable heights of the adsorbed Pb islands, the measured STS spectra of the quantum well states[61] as well as lifetimes of the QWSs with energies up to 3 eV with respect to the Fermi level.[45] The details of the potential construction are given elsewhere.[61,62] We then briefly comment on the most important features of the model relevant for the present study.

The stabilized jellium description is used for the Pb overlayer. The calculated bulk Pb work function value ($\Phi = 4.08$ eV) is consistent with *ab initio* calculations[17,18,63] and with experimental data.[20,64,65] The Cu(111) substrate is represented with pseudopotential built on the basis of a 1D model potential only function of the electron coordinate z perpendicular to the surface.[66] The model potential of Ref. 66 is adjusted to the Cu(111) band structure at $\bar{\Gamma}$ (energy of the ISs, energy of the surface state, energy position of the projected band gap). In our particular implementation,[62] the L gap of Cu(111) confining the QWSs in Pb/Cu(111) extends from -1.02 to $+4.12$ eV with respect to the Fermi level. By construction the system has translational invariance in the surface (x,y) plane. The single-particle orbitals are then sought in the form

$$\Psi_{m\mathbf{k}}(\mathbf{r}) = \psi_m(z)e^{i\mathbf{k}\cdot\mathbf{r}_\parallel}, \tag{3}$$

where $\mathbf{k}$ is the electron wave vector parallel to the surface and $\mathbf{r}_\parallel = (x,y)$. The orbitals $\psi_m(z)$ are the solutions of the 1D Kohn-Sham equations obtained for a periodic symmetric supercell comprising a Cu(111) slab of 25 Cu(111) layers covered on both sides by Pb overlayers and 30–40a_0-thick vacuum layers. Observe that the quantum number m in Eq. (3) is running over all Cu-substrate (delocalized) and Pb-overlayer (localized) states according to their energy at $\bar{\Gamma}$. One can ascribe a quantum number [we will denote it as j in what follows] specific to the QWSs based on their nodal structure outside the Cu(111) slab.[45]

It is well known that the DFT-LDA scheme does not reproduce the long-range image potential interaction between an electron placed in vacuum in front of a metal surface. This interaction is of paramount importance for the present study focused on the electronic states with partial IS character at low binding energies close to the vacuum level. Following the strategy developed in Ref. 61, the self-consistent one-electron potential $V_{\text{eff}}(z)$ resulting from the DFT-LDA calculations of Pb/Cu(111) has been corrected by smoothly matching the classical image potential above the Pb overlayer. The resulting one-electron potential has the form:

$$V_s(z) = \begin{cases} \frac{A\exp[-\lambda(z-z_0)]-1}{4(z-z_{\text{im}})}, & z \geqslant z_0, \\ V_{\text{eff}}(z), & z_{5\text{ML}} \leqslant z < z_0, \\ V_{\text{Cu}}(z), & z_c \leqslant z < z_{5\text{ML}}. \end{cases} \tag{4}$$

For an electron in vacuum $z \gg z_{\text{im}}$, Eq. (4) converges to classical image potential $-1/4(z - z_{\text{im}})$. The potential $V_s(z)$ is set symmetric with respect to the center of the Cu(111) slab z_c. The image plane position is given by z_{im}, and z_0 is the matching position parameter. We take $z_{\text{im}} = 1.23a_0$ in front of the Pb jellium edge,[67] and z_0 is set to $z_0 = z_{\text{im}} + 1.0a_0$, which gives a smooth potential. Parameters A and λ are fixed by the continuity of $V_s(z)$ and its derivative $V_s'(z)$ at z_0. Since

the top edge of the Cu(111) gap lies close to the vacuum level, we have extended the Cu(111) slab to properly account for the penetration of the QWSs with IS character inside the substrate. The Cu(111) layers described with the model potential[66] $V_{\mathrm{Cu}}(z)$ have been inserted into the slab below the fifth Cu atomic monolayer (ML) at $z_{5\mathrm{ML}}$. Indeed, well inside Cu(111) the overlayer appears screened and $V_{\mathrm{eff}}(z)$ converges to the oscillatory part of the model potential of Ref. 66. Because of the image potential, the electronic states with energies close to the vacuum level extend far outside the metal slab. Consequently, to guarantee good description of these states, we have added a large vacuum space of $200a_0$ on both sides above the Pb surfaces.

With the supercell method described above we have calculated confined states with energies up to −50 meV with respect to E_V. It is noteworthy that with changing Pb coverage the work function oscillates with respect to the converged value (≈4.08 eV above 12 ML). This quantum size effect is particularly noticeable for the smaller thicknesses below 5–6 ML, with work function oscillation amplitude of the order of 0.2–0.1 eV. The top edge of the projected Cu(111) gap can then appear below the vacuum level so that the Pb localized states at small binding energies $E - E_V$ turn into resonances. The resonant states have not been addressed here.

B. Many-body calculation of the decay rates.

Detailed experimental and theoretical studies of the lifetimes of the ISs and QWSs have shown that parameter-free many-body calculations allow nowadays quantitative description of the inelastic electron-electron decay rates.[29,38,53] We use a well established approach where the electron-electron decay rate of excited states is performed at $\bar{\Gamma}$ point ($\mathbf{k}_\parallel = 0$) by projecting the imaginary part of the self-energy onto the corresponding wave function.[30,45] In the present symmetry, we have

$$\gamma^{j}_{e\text{-}e} = -2 \iint dz dz' \psi^*_j(z) \mathrm{Im}\Sigma(z,z';0,E_j)\psi_j(z'), \qquad (5)$$

where E_j is the energy of the surface-localized Kohn-Sham orbital ψ_j, and $\Sigma(z,z';\mathbf{k}_\parallel,\omega)$ is the 2D Fourier transform of the self-energy. Based on the one-electron eigenstates of the system described with the potential given by Eq. (4), the nonlocal self-energy is evaluated in the GW approximation, as detailed in Refs. 53,68. *A priori*, the GW correction to the one-particle energies of the QWSs can be also obtained within a similar scheme. However, the model Cu(111) potential[66] has been adjusted to the theoretical and experimental data with DFT-LDA calculations so that performing GW correction to the energies of the QWSs would be inconsistent with the description of the Cu(111) substrate.

The many-body calculations of the decay rates are computationally demanding because of the large size of the supercell required to account for the excited state spill out from the surface due to the QWS/IS hybridization. We then have used the GW approximation to obtain $\gamma^{j}_{e\text{-}e}$ for some of the QWS/IS states. These have been used to validate a simpler wave packet propagation (WPP) and wave-function penetration[12,51] description of the decay. Both are closely related through the assumption of the locality of self-energy Σ and give the same result within the first-order perturbation theory.[61]

C. Wave packet propagation study of the excited electron dynamics

The WPP consists in the direct solution of the time-dependent Schrödinger equation (TDSE) discretized on a spatial grid. The method is discussed in great detail in Ref. 30. In the present case, because of the translation invariance in the surface plane, we are interested only in the characteristics of the excited states at the $\bar{\Gamma}$ point. The 1D-TDSE then reads

$$i\partial_t\phi(z,t) = \left[-\frac{1}{2}\frac{\partial^2}{\partial z^2} + U(z) + V_{\mathrm{abs}}(z)\right]\phi(z,t). \qquad (6)$$

Provided the initial condition $\phi(z,t=0) = \phi_0(z)$, Eq. (6) is solved with the short-time propagation and split-operator technique.[69]

The effective local one-electron potential U describes the interaction of the "active" electron with the Pb/Cu(111) system. It is given by the sum of the electron-surface interaction V_{s} and the non-Hermitian term $V_{e\text{-}e}$, allowing to account for the excited state population decay via inelastic electron-electron scattering:

$$U(z) = V_{\mathrm{s}}(z) + V_{e\text{-}e}(z). \qquad (7)$$

The electron-surface interaction V_{s} is essentially that given by Eq. (4), but with the crucial difference that only one vacuum/Pb/Cu(111) interface is considered and the semi-infinite Cu(111) substrate is implemented by (i) imposing $V_{\mathrm{s}}(z) = V_{\mathrm{Cu}}(z)$ for $z < z_{5\mathrm{ML}}$ and (ii) introducing the absorbing potential $V_{\mathrm{abs}}(z)$ at the grid boundary inside Cu(111) to suppress the reflections of the wave packet.[70]

Inclusion of the non-Hermitian potential $V_{e\text{-}e}$ is similar to the approach used in theoretical low-energy electron diffraction studies.[71] This potential is defined in such a way that the first-order perturbation estimate for the inelastic decay rates of the QWSs localized inside Pb overlayer give the bulk decay rate in agreement with many-body calculations.[35,37,38,45] In practice $V_{e\text{-}e}$ is set with respect to the Pb jellium edge $z_{\mathrm{jel}} = z_{\mathrm{im}} - 1.23a_0$ as[61]

$$V_{e\text{-}e} = -i\frac{\gamma^{\mathrm{bulk}}_{e\text{-}e}}{2}\frac{1}{1+e^{(z-z_{\mathrm{jel}})/\delta}}. \qquad (8)$$

The parameter of the switching function is $\delta = 0.09a_0$. The inelastic decay rate of an electronic state confined in the bulk Pb metal $\gamma^{\mathrm{bulk}}_{e\text{-}e}$ has been taken from Ref. 45. It should be emphasized that $\gamma^{\mathrm{bulk}}_{e\text{-}e}$ strongly depends on the energy of the excited state. The higher is the energy of the excited state with respect to the Fermi level, the shorter is the corresponding lifetime. This implies that for WPP calculation of the QWS/ISs the contribution $\gamma^{\mathrm{bulk}}_{e\text{-}e}$ in Eq. (8) has to be adjusted to the energy interval under study.

Once the solution $\phi(t)$ is obtained, the autocorrelation function $\langle\phi_0|\phi(t)\rangle$ can be used to extract all the properties of interest, such as energies and lifetimes of the decaying quasistationary states of the system as well as the projected density of states (PDOS).[30]

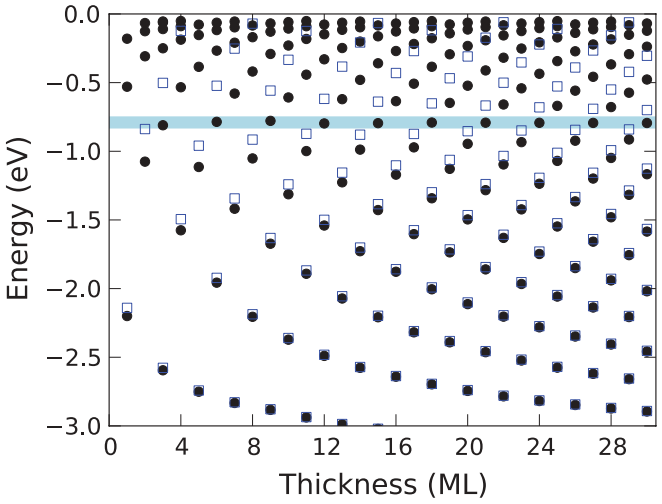

FIG. 1. (Color online) Calculated energies of the QWSs as a function of the overlayer thickness for the Pb/Cu(111) system. Results are shown for the calculations performed with (black dots) and without (open squares) inclusion of the image potential tail in the DFT potentials. Energies E_n are referred to the vacuum level. The energy with respect to the Fermi level of the thick Pb film is $E_n + 4.08$ eV, where 4.08 eV is the work function of Pb. The horizontal shaded area denotes the set of states lying at energy ≈ -0.8 eV.

III. RESULTS AND DISCUSSION

A. Electronic structure

The discussion is started by revisiting the electronic structure of the Pb/Cu(111) system (see Ref. 61). We focus on the previously uncovered energy region −3–0 eV with respect to the vacuum level, where the image potential tail becomes progressively important. Figure 1 shows the energies of the QWSs calculated up to −0.05 eV as a function of the Pb overlayer thickness varied within 1–28 ML range. Results obtained with the model potential given by Eq. (4) are compared with those obtained with DFT-LDA effective potential only,[61] i.e., without accounting for the image potential tail of the electron-surface interaction. For the states below −2 eV with respect to the vacuum level, the two sets of results coincide. Being well localized inside the Pb overlayer, these states are not sensitive to the potential change above the surface. The energies form a particle-in-a-box sequence usually considered for the QWSs. At variance, close to the vacuum level, the two sets of results are different. The DFT-LDA potentials vanish exponentially into the vacuum side, and allow only for a finite number of states to be accommodated in the potential well. Inclusion of the long-range image potential tail of electron-surface interaction allows for the QWSs hybridization with ISs. As a result, an infinite (Rydberg) series of states converging toward the vacuum level exist for each thickness.

As another interesting feature, it follows from Fig. 1 that a state with an energy ≈ -0.8 eV with respect to the vacuum level systematically appears every 3 ML at coverages of 3, 6, 9,... ML. For the stabilized jellium description of Pb as used here, the wavelength of an electron moving inside the film with −0.8 eV energy is $\lambda \approx 6a/5$, where a is the interlayer spacing ($a = 5.41a_0$). This regularity is similar to the series of unoccupied QWSs observed in Pb overlayers close to the Fermi level E_F, at $E - E_F \approx 0.65$ eV, which appear for an even number of ML. In the latter case, however, the states are characterized by $\lambda \approx 4a/3$. In good agreement with our theoretical findings, in the TR-2PPE study of the Pb/Si(111) system[38] a QWS/IS hybrid state has been observed at −0.79 eV with respect to the vacuum level. However, Kirchmann *et al*. reported this state for all overlayer thicknesses,[38] while in our calculations it appears only every 3 ML. The origin of this discrepancy is unclear at the moment. Indeed, the exact energy of the QWS/IS hybrid state depends on the overlayer thickness, as shown in Ref. 47 and discussed below.

The semiclassical phase accumulation model[12,13] allows quantitative analysis of the results discussed above. Within this model the energy of the discrete state E_j is determined from the quantization condition on the total phase acquired by an electron on the closed trajectory inside the potential well:

$$2\pi j = 2kD + \varphi_b + \left[\frac{\pi}{\sqrt{8(E_V - E_j)}} - \pi\right], \qquad (9)$$

where the term in the brackets is the phase due to the electron scattering on the image potential[72] at the vacuum side. The phase accumulated by the electron on the round trip inside the Pb overlayer is given by $2kD$, where $D = Ja$ is the thickness of the Pb overlayer comprising J monolayers. Within the present jellium description of the Pb film, the electron momentum perpendicular to the film surface is $k = \sqrt{2(E_j - U_0)}$, where U_0 is the bottom of the valence band (−13.55 eV for the thick layer with work function of bulk Pb). Finally, φ_b stands for the phase shift due to electron scattering at Pb/Cu(111) interface and Pb film surface region characterized by the transition from the bulk Pb to the image potential for the excited electron. With substitution $k = 2\pi/\lambda$, we obtain that for the electron wavelength $\lambda \approx 6a/5$ the term $2kD$ changes by 10π for $\Delta J = 3$, i.e., adding 3 ML does not change the energy of the state located at ≈ -0.79 eV, but adds five zeros to the nodal structure of the wave function inside the film. For the QWSs with high binding energies well below the vacuum level, one retrieves the well documented quantization condition $2\pi j = 2kD + \delta$ with δ slowly varying function of electron energy.

Close to the vacuum level, the phase will be determined by the divergence in image potential phase shift for $E_j \to E_V$. Using notation $\varphi_b - \pi \equiv 2\pi\chi$, Eq. (9) can be transformed to the form

$$E_V - E_j = \frac{1}{32(j - 2D/\lambda - \chi)^2}. \qquad (10)$$

Finally, writing $2D/\lambda - \chi = l - \alpha$ with l being the number of zeros of the wave function (half electron wavelength) inside the film, we arrive to

$$E_V - E_j = \frac{1}{32(j - l + \alpha)^2}. \qquad (11)$$

Close to E_V, the change of the electron wave vector k is very small on the energy scale given by the fast variation of the image potential phase shift. Thus, l and α can be considered as energy independent, however, these parameters are specific for the overlayer of a given thickness. Comparing Eq. (11)

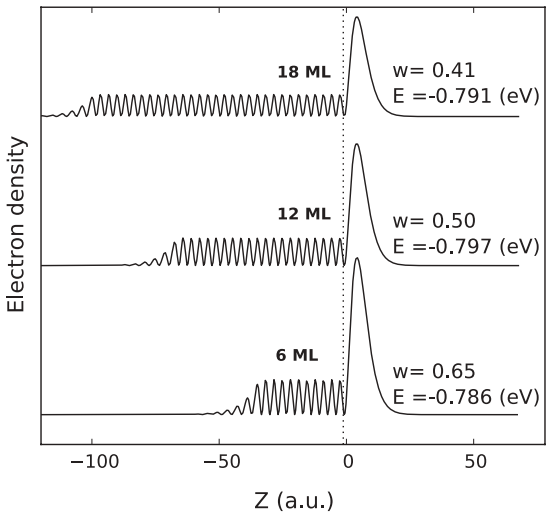

FIG. 2. Electron densities of the hybridized QWS/ISs with energy ≈ -0.8 eV with respect to the vacuum level (see horizontal shaded area in Fig. 1). Results for the 6, 12, and 18 ML-thick Pb films on Cu(111) substrate are shown as a function of z coordinate perpendicular to the surface of the film. For each state, the energy E and weight in the vacuum region w are indicated. The origin $z = 0$ is placed at the image plane position and the vertical dotted line at $z = -1.23a_0$ denotes the jellium edge.

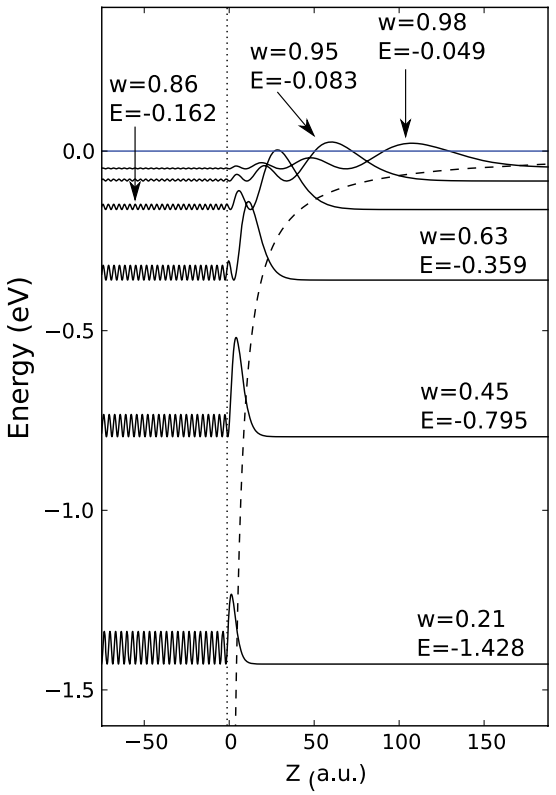

FIG. 3. (Color online) Electron densities of the hybridized QWS/ISs with different energies approaching the vacuum level $E_V = 0$. Results for the 15 ML-thick Pb film on Cu(111) substrate are presented as a function of z coordinate perpendicular to the surface of the film and measured from the Pb image plane. The z-distance range is zoomed at the Pb/vacuum interface to show the IS contribution to the wave functions. The results are vertically offset according to the energy of the corresponding state with respect to the vacuum level denoted by a horizontal line. Dashed line represents the image potential and the vertical dotted line at $z = -1.23a_0$ denotes the jellium edge. For each state, the energy E and weight in the vacuum region w are indicated.

with Eq. (2) describing the energies of the ISs, it is natural to associate $n_j = j - l$ with an effective IS quantum number reflecting the nodal structure of the wave function on the vacuum side. The parameter α corresponds then to the quantum defect, which is dependent on the overlayer thickness. Thus close to the vacuum level QWSs mix with ISs and acquire an IS character, where each next quantized state corresponds to a zero of the wave function appearing on the vacuum side.

In Figs. 2 and 3, we show the electron densities of the hybridized QWS/ISs calculated for Pb overlayers on Cu(111). The states presented in Fig. 2 are all characterized by a binding energy ≈ -0.8 eV. This allows transparent discussion of the dependence of the properties of the hybridized states on the overlayer thickness for a fixed energy. Since the energy is fixed, the overall shape of the wave function is preserved. In particular, for different overlayer thicknesses, the electron density shows a pronounced maximum on the vacuum side at essentially the same z position. It manifests a strong contribution of the first image potential state into the hybrid state. The damped oscillations on the left of the quantum well correspond to the finite penetration of the wave function into Cu(111) substrate. These are typical for the states with energies within the projected band gap of Cu(111). Each increase of the film thickness by 3 ML extends the wave function inside Pb overlayer by five semiperiods. As a consequence, the probability to find an electron on the vacuum side shows a quantum size effect decreasing with increasing film thickness. The weight of the wave function on the vacuum side $\mathrm{w} = \int_0^\infty |\psi|^2 dz$ ($z = 0$ corresponds to the image plane position) decreases progressively from 0.65 to 0.41 for the considered 6–18 ML coverage range. As we will show below, this effect has direct consequences on the lifetime of the excited states.

Figure 3 shows the evolution of the electron densities of the hybrid QWS/ISs with their binding energy for 15 ML Pb/Cu(111). As the energies of the QWSs approach the vacuum level, the vacuum part of the corresponding wave functions acquires an IS character. The weight of the wave function in vacuum rapidly increases and the characteristic nodal structure is developed above Pb surface.[47] In agreement with Eq. (11), for energies $E_j > -0.125$ eV, each next state $n \to n + 1$ is associated with an additional zero located on the vacuum side while the nodal structure inside the Pb overlayer is unchanged. Tracing $(32|E_j|)^{-1/2}$ as a function of the quantum number allows to determine the leading contribution of the ISs with $n_j = j - l = 2$, 3, and 4 into the QWS/IS hybrids with energies -0.162, -0.083, and -0.049 eV, respectively. The states at -0.795 and -0.359 eV both show the leading contribution of the $n_j = 1$ IS. It should be stressed that, despite the strong IS character of the states, their precise binding energy is determined by the penetration of the wave function into the overlayer.

B. Decay rates of hybrid QWS/ISs

1. Qualitative discussion

As follows from the energies and wave functions of the hybrid QWS/ISs discussed above, the QWS hybridization with ISs results in the partial transfer of the electron density into the vacuum above the surface of the Pb overlayer. Thus an excited electron appears less coupled with electronic excitations in the metal, which should increase its lifetime. Prior to showing the calculated decay rates, we would like to develop here a simple semiquantitative approach based on the wave-function penetration.[12,29,51] Analogous to the phase accumulation model for the energies of excited states, the wave-function penetration based estimate for $\gamma^j_{e\text{-}e}$ allows one to obtain closed-form analytical expressions, useful in analyzing the results of numerical studies and predicting the dependence of many-body decay rates on different parameters.

The penetration approach grounds on the assumption that the excited electron undergoes inelastic scattering with electrons from the Fermi sea mainly inside the metal bulk, and that the self-energy is local. The decay rate of a given state with energy E_j can be then estimated from the first-order perturbation theory as the value of the bulk decay rate $\gamma^{\text{bulk}}_{e\text{-}e}$ at the same energy E_j weighted by the penetration of the wave function into the metal:

$$\gamma^j_{e\text{-}e} = \gamma^{\text{bulk}}_{e\text{-}e} \frac{\int_{-\infty}^{0} |\psi_j(z)|^2 dz}{\int_{-\infty}^{\infty} |\psi_j(z)|^2 dz}, \tag{12}$$

where $z = 0$ is taken at the Pb image plane position. In Ref. 53, it has been shown that since the nonlocality of the electron self-energy is neglected, the linewidths of the ISs at clean metal surfaces are underestimated as compared to the GW results. However, in many cases, such as rare gas adsorption on metal surfaces, Eq. (12) appears to quantitatively reproduce the experimental data.[29,51]

In the case of the Pb overlayers on Cu(111) surface, for an electron excited in the hybrid QWS/IS, the probability $\mathrm{p} = 1 - \mathrm{w}$ to reside inside the Pb overlayer is given by

$$\mathrm{p} = \frac{\int_{-D}^{0} \cos^2(kz+\xi) dz}{\int_{-D}^{0} \cos^2(kz+\xi) dz + \mathcal{C}^2 \int_{0}^{\infty} z^2 R^2(n_j, z) dz}, \tag{13}$$

where $\cos(kz+\xi)$ is the electron wave function inside the overlayer with wave vector k and phase ξ. The hydrogenic wave function $R(n_j,z)$ stands for the vacuum part of the IS wave function and describes an electron, with principal quantum number n_j and zero angular momentum, moving in the field of a point charge of value $+1/4$. The quantum number n_j of the IS giving leading contribution to the discrete state j is defined by Eqs. (10) and (11). The constant $\mathcal{C}$ arises from matching solutions at the film/vacuum interface. In deriving Eq. (13), because of the exponential wave-function damping inside the projected band gap, we have neglected the contribution of the Cu(111) substrate. We have also neglected the contribution of the transition region between the vacuum side characterized by the image potential for the electron surface interaction and the inside of the Pb overlayer. Performing integrations in Eq. (13), we arrive at

$$\mathrm{p} = \frac{D - \sin(kD)\cos(kD - 2\xi)/k}{D - \sin(kD)\cos(kD - 2\xi)/k + \beta n_j^3}, \tag{14}$$

where β is a constant.

For the states close to the vacuum level, $D \gg 1/k$ and the corresponding terms can be neglected in Eq. (14). This leads to the following perturbative estimate for the inelastic electron-electron scattering contribution to the excited-state decay:

$$\gamma^j_{e\text{-}e} = \gamma^{\text{bulk}}_{e\text{-}e} \frac{D}{D + \beta n_j^3}. \tag{15}$$

In the narrow energy range close to the vacuum level, which is of relevance for the QWS/IS hybridization, the variation of $\gamma^{\text{bulk}}_{e\text{-}e}$ is small. The decay rates of the hybrid states $\gamma^j_{e\text{-}e}$ should then display two main trends. (i) For the fixed thickness D of the Pb overlayer the decay rate drops as the energies of the states approach the vacuum level. For large effective quantum numbers n_j, one expects $\gamma^j_{e\text{-}e} \sim 1/n_j^3$ behavior typical for the ISs,[12,29,50–54] and well understood as resulting from the fact that the excited electron mainly resides in vacuum far from the surface. (ii) For the fixed effective quantum number n_j, the decay rate increases with increasing D and asymptotically reaches the $\gamma^{\text{bulk}}_{e\text{-}e}$ value. This is physically sound since for the very thick overlayers the excited electron is entirely localized inside Pb.

The above analysis is fully supported by the results of the calculations presented below. It should be noted that the perturbative approach above neglects the nonlocal effects in the self-energy and the decay is only considered inside the metal. Within this approximation, the WPP method offers an exact treatment of the decay rates of the QWS/ISs. The effective many-body absorbing potentials here are defined from $\gamma^{\text{bulk}}_{e\text{-}e}$ as explained in Sec. II. In this approach, different absorbing potentials can be ascribed to different metallic regions. In the following analysis, inside the Pb overlayer, we have used the bulk decay rates derived from GW calculations in Ref. 45. Inside Cu substrate, the Quinn-Ferrell[73] quadratic dependence of the decay rate on the electron energy $\gamma^{\text{bulk}}_{e\text{-}e} = 29.1(E[\text{eV}] - E_F[\text{eV}])^2$ meV has been used. The effect of using a different decay rate inside Cu, and more generally, of accounting for inelastic many-body effects inside Cu is small because of the band gap effect leading to small wave-function penetration into the substrate.

2. Calculated decay rates

Figure 4 shows the calculated inelastic decay rates of the hybrid QWS/ISs as a function of the thickness of the overlayer and the energy of the state. Basically, the results displayed in panels (a) and (b) of the figure confirm predictions drawn from the simple analysis given by Eq. (15). We start the discussion with the results of the decay rate dependence on the overlayer thickness for fixed QWS energy. This is possible due to appearance of the state lying at ≈ -0.8 eV with respect to E_V each 3 ML of Pb coverage in the 3, 6, 9, ... ML sequence. The effective quantum number of the IS contributing to the hybrid is $n_j = 1$ in this case. The corresponding results are presented in Fig. 4(a). This figure also allows one to quantify the difference between state-of-the-art many-body GW calculation of the

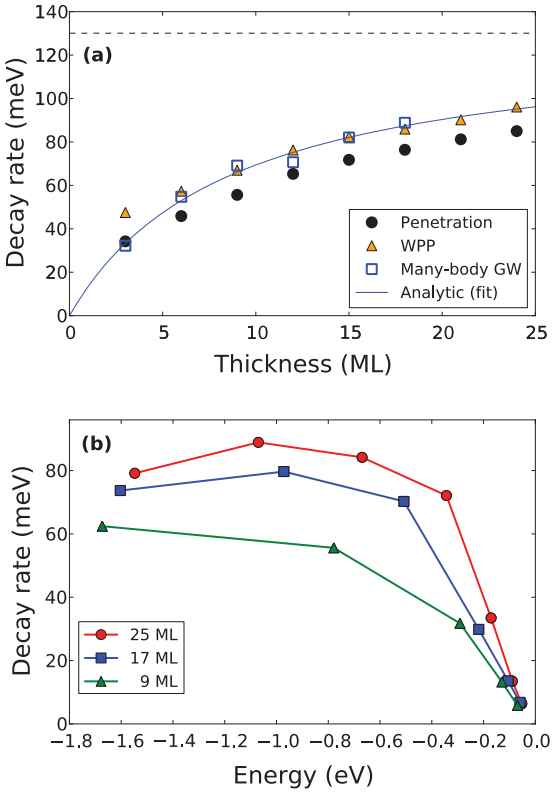

FIG. 4. (Color online) (a) Calculated many-body $\gamma^j_{e\text{-}e}$ decay rates of the states lying at -0.8 eV as a function of overlayer thickness. Open squares: many-body GW results. Triangles: WPP results. Dots: decay rates calculated from the wave-function penetration. Solid line: fit to the GW data with Eq. (15) (see main text for details). The horizontal dashed line at 130 meV denotes the theoretical bulk decay rate for the energy -0.8 eV. (b) Decay rates $\gamma^j_{e\text{-}e}$ of the hybridized QWS/ISs as calculated from the wave-function penetration with Eq. (12) for 9, 17, and 25 ML-thick Pb overlayers on Cu(111). Results are shown as a function of the energies of the states measured with respect to the vacuum level.

$\gamma^j_{e\text{-}e}$ decay rates and more simple approaches. In this respect, it is noteworthy that the GW results closely agree with WPP and wave-function penetration [see Eq. (12)] treatments.

The calculated decay rates are strongly reduced with respect to the 130 meV value expected for a state at the same energy located inside the Pb overlayer. In the 3 ML coverage case, a decay rate as low as 32 meV is obtained, which is of the order of the decay rates of image states at noble metal surfaces.[52,53] This is fully consistent with the low penetration ($p = 0.25$) of the hybrid QWS/IS into the metal. With increasing Pb coverage, decay rates increase showing a strong quantum size effect as predicted by Eq. (15). Basically, the decay rate is doubled when Pb coverage increases from 3 to 15 ML. Assuming $\gamma^{\text{bulk}}_{e\text{-}e} = 130$ meV, $D = Ja$, where J is the number of monolayers and a the interlayer distance, $n_j = 1$, and considering β as a free parameter, Eq. (15) provides a remarkable fit to the GW data [see solid line in Fig. 4(a)].

The fact that the simple approach based on the wave-function penetration can describe the GW results with a precision of 20%, supports its use for different energies of the excited states and different overlayer thicknesses. This allows to cover a broad range of these parameters with low computational cost as compared to the GW calculations. This holds especially true for thick overlayers and high n_j states. For some states, different from those shown in Fig. 4(a), we have additionally checked with GW that the perturbative analysis holds valid from the semiquantitative point of view.

In Fig. 4(b), we show the dependence of the decay rates of the hybrid QWS/ISs on their energies for three Pb films of thicknesses 9, 17, and 25 ML. Results are obtained from the wave-function penetration. In agreement with the preceding discussion and analysis based on Eq. (15), the decay rates increase in overall when increasing the overlayer thickness. For the fixed thickness of the Pb film, when the energies E_j of the excited states approach the vacuum level, the calculated decay rates decrease. As seen in Fig. 3, the electron is pushed away from the metal surface, reflecting hybridization with high n ISs. The calculated $\gamma^j_{e\text{-}e}$ then drops as $1/n_j^3 \propto |E_j|^{3/2}$, consistent with Eq. (15). QWS/IS hybrids recover a well documented behavior for the ISs lifetimes on the pristine surfaces of noble metals.

Figure 5 summarizes present and earlier results[45] for the inelastic electron-electron decay rates of the QWSs in Pb/Cu(111). The decay rates of different states are shown as a function of their energy, measured with respect to E_V. A broad range of Pb overlayer thicknesses is encompassed in the figure: up to 28 and 18 ML for present and earlier results, respectively. Such synthetic representation makes the effect of the QWSs hybridization with ISs particularly apparent. The energy scale extends from the Fermi level to the vacuum level, where calculations have been performed for the states with energies up to -50 meV. The many-body GW results of Ref. 45 (GW-LDA) correspond to the description of the Pb overlayer with effective one-electron potential derived within the local density approximation of density functional theory. No image potential effect has been included. Present calculations include the image potential tail of the electron-surface interaction and so allow for the QWSs hybridization with ISs.

The QWSs with low excitation energies are localized inside the Pb overlayer and are insensitive to the inclusion of the image potential tail of the electron-surface interaction. The decay rates of these states are basically equal to the decay rates of electronic excitations in bulk Pb and display the "standard" behavior with excitation energy. With increasing energy $\gamma^j_{e\text{-}e}$ increases following the quadratic Quinn-Ferrell[73] dependence $\gamma^j_{e\text{-}e} \approx \gamma^{\text{bulk}}_{e\text{-}e}(E_j) = \epsilon(E - E_F)^2$, as found in several studies performed on metallic overlayers with time-resolved photoemission and scanning tunneling spectroscopy. The *ab initio* studies[46] performed for bulk Pb quantitatively confirm present results based on the free-electron description of Pb.

At large excitation energies $E - E_F > 2.5$ eV, or equally $E - E_V > -1.5$ eV, inclusion of the image potential tail has dramatic consequences on the decay rates of the QWSs. The GW-LDA decay rates continue to increase with energy, basically reflecting the energy dependence of the bulk decay rates. In contrast, present results show a crossover: at the energy around $E - E_V \sim -1$ eV, the decay rates of QWSs first level off and then quickly decrease for energies close to the vacuum level E_V. The crossover at ~ -1 eV reflects the onset of the QWSs hybridization with ISs. The states acquire a partial IS character with electron density being pushed away from the

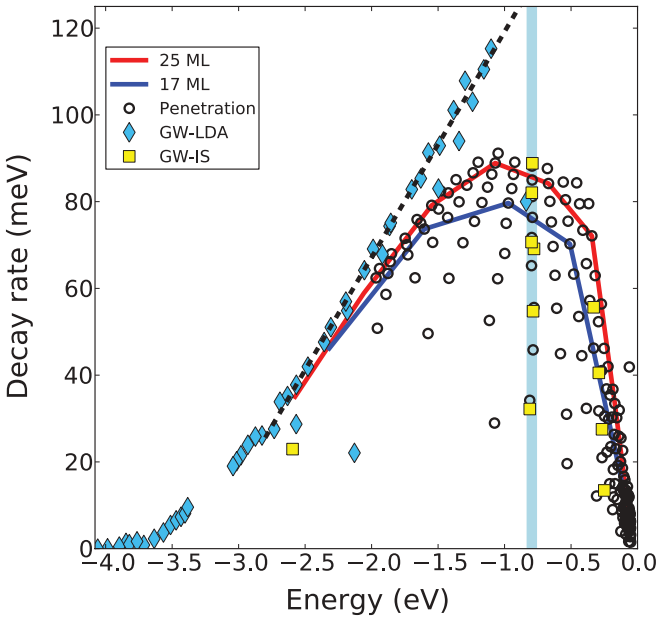

FIG. 5. (Color online) Calculated many-body $\gamma^{j}_{e\text{-}e}$ decay rates of the hybrid QWS/ISs for overlayer thicknesses ranging from 1–28 ML. Results are shown as a function of the energy of the states as measured with respect to the vacuum level. Thick solid lines connect the decay rates for a few selected overlayer thicknesses (see the legend). Thin dashed line represents the linear fit to the dispersion of the decay rates of the QWSs obtained in an earlier work[45] without accounting for the image potential tail of the electron-surface interaction. Different symbols are explained in the legend. Penetration stands for the present calculations based on the wave-function penetration. These calculations account for the image potential tail of the electron-surface interaction. GW-LDA stands for the decay rates calculated within GW approach and effective one-electron potential derived within the local density approximation of density functional theory where the image potential is not accounted for. GW-IS stands for the decay rates calculated within GW approach and effective one-electron potential, corrected such that the image potential tail of the electron-surface interaction is accounted for. The vertical shadowed region represents the narrow energy window of the shadowed area of Fig. 1 at ≈ -0.8 eV.

metal into the vacuum. This stabilizes the corresponding state and the decay rate drops as predicted by Eq. (15), which has been also analyzed in relation with Fig. 4(b). The accumulation of data points close to the vacuum level in Fig. 5 reflects the high number of states in this energy region (see also Fig. 1), consistent with the formation of the Rydberg series. In overall, the decay rates are smaller for smaller coverages in this energy region [see also Fig. 4(a)]. This is directly linked to the previously discussed quantum size effect and can be also inferred from Eq. (15).

At this point it is interesting to compare present results with those obtained for the dielectric spacer (rare gas) overlayers, where the hybridization between ISs and QWSs localized in the conduction band of the dielectric overlayer has also been reported.[50,51,55–60] However, in the case of dielectric spacer layers, the lifetimes of excited states show the dependence on the overlayer thickness distinct from the present results. Thus, for Xe/Ag(111) the decay rates of the $n = 2$ and $n = 3$ ISs hybridized with QWSs show an oscillating structure with increasing Xe coverage.[51,55–57] Similar results were reported for Kr/Cu(100) and Xe/Cu(100).[51] This is in contrast to the smooth increase of many-body decay rates with overlayer thickness as reported here for Pb/Cu(111).

Different dependence of the excited electron dynamics on the overlayer thickness for metal and dielectric overlayers can be explained as due to the difference in their electronic structure and excitation relaxation pathways. For the metal films, the potential well is deep so that many occupied and empty QWSs are accommodated even at small film thicknesses. The excited state population mainly decays via electron-electron interactions inside the film,[38,45] in contrast with rare-gas adlayers, where the excited state population decays via interaction with substrate electrons. The dielectric rare gas Xe (Kr) layer forms a shallow potential well with conduction band minimum at -0.55 eV with respect to the vacuum level. This potential well can host only a small number of QWSs. For 6 ML of Xe on Ag(111), one unoccupied QWS is formed with energy close to the vacuum level and hybridizes with $n = 2$ and $n = 3$ ISs.[51,55–57] Because of the shallow potential well, the wave vector k is small and the $\sin(kD)\cos(kD - 2\xi)/k$ terms in Eq. (14) cannot be neglected. The wave-function penetration into the overlayer and its overlap with the substrate show then a pronounced increase as soon as an integer number of electron half-wavelength can be hosted inside the rare-gas film. This explains the oscillating structure in the dependence of the decay rates of the hybrid states on the rare gas overlayer thickness, not observed here with metallic Pb overlayer.

C. Thick overlayer limit

As follows from Eq. (15), with increasing overlayer thickness, the hybrid QWS/ISs with energies very close to the vacuum level will retrieve the bulk decay rate $\gamma^{\mathrm{b}}_{e\text{-}e}$ irrespective of how large the effective quantum number n_j is. The increase in decay rates will be accompanied by the decrease in the energy separation between the states. From the point of view of the underlying physics, the excited electron launched from the surface of the overlayer into the bulk, even if it reaches the Pb/Cu(111) interface and is back reflected, decays before reaching the surface of the film. The evolution of the excited electron population at the surface is then the same as in the bulk Pb case.

The above point is illustrated with Fig. 6. The projected density of states calculated with WPP is shown as a function of energy for some selected overlayer thicknesses. We have used Gaussian wave packets of the form $\phi_0(z) = \exp[-(z - z_0)^2/\Delta^2]$ placed at the Pb-vacuum interface. The absorbing potential has been set from the theoretical electron-electron decay rate in the metal: $\gamma^{\mathrm{b}}_{e\text{-}e} = 130$ meV at energy $E = -0.8$ eV. Figure 6 nicely shows a transition from a peak structure with well resolved QWSs to the limit of the surface of the semi-infinite Pb metal. Basically, above the thickness of $D = 60$ ML the quantization of the electronic states in Pb/Cu(111) cannot be resolved. Note that in experiments, this limit is expected to be reached at lower thicknesses because of the additional decay channels [see Eq. (1)] contributing to the broadening of the states.

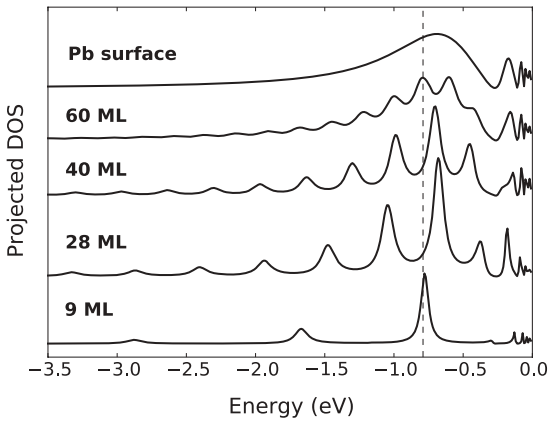

FIG. 6. Projected density of states (arbitrary units) at the Pb surface in Pb/Cu(111) system. Results are obtained with WPP method for different Pb overlayer thicknesses, as indicated above the corresponding lines. The limit of the infinite thickness is indicated as Pb metal surface. The data are vertically offset for clarity.

IV. SUMMARY AND CONCLUSIONS

In summary, on the example of Pb overlayers on Cu(111), we have studied the hybridization between metal overlayer localized quantum well states and image potential states at energies close to the vacuum level. Calculations performed over a broad range of overlayer thicknesses allow a detailed discussion of how the QWS/IS hybridization affects the lifetimes of excited states and how this effect depends on the overlayer thickness. For the hybridized QWS/ISs, the rate of the inelastic decay via electron-electron scattering has been obtained using several approaches: (i) GW calculations, (ii) one-electron wave-packet propagation (WPP) studies with model absorbing potentials inside the film, and finally, (iii) first-order perturbation theory based on the wave-function penetration. This allows us to explain the calculated trends as originating from the different overlap of the QWS wave function with the overlayer/substrate metal.

We have found that close to the vacuum level, properties of the excited electronic states of the metallic overlayers are determined by the hybridization between the QWSs and ISs. The electron density is shifted away from the metal, and both the energies and the many-body decay rates of the states are affected.

(1) The particle-in-a-box energy progression of the QWSs holds only up to some energy (typically from -1.5 to -2 eV with respect to the vacuum level). At higher energies close to the vacuum level the infinite Rydberg series of states typical for the ISs is formed. The precise value of the energies (or quantum defect) is determined by the film thickness, as has been already pointed out in Ref. 47.

(2) The many-body decay rates of the states show a pronounced change in the energy dependence when approaching the vacuum level. The bulklike increase of the decay rate with increasing QWS energy E_j is saturated at some point and changes to the decreasing $\propto(E_V - E_j)^{3/2}$ behavior typical for the ISs. The crossover corresponds to the shift of the excited electron wave-function weight from inside the Pb metal into the vacuum and depends on the Pb overlayer thickness.

(3) For the fixed energy of the QWS/IS hybrid state, the many-body decay rate increases with increasing overlayer thickness, since the probability to find an excited electron inside the overlayer grows. In the limit of thick overlayer, the bulk decay rate is retrieved. This holds always, independently of the energy of the state. However, the closer is the state to the vacuum level, the thicker should be the Pb quantum well to shift the wave-function weight from the vacuum into the metal.

With the phase accumulation model and wave-function penetration approach, we obtained an analytical description of the above results. In particular, simple asymptotic forms have been defined for the energies of the states close to the vacuum level as well as for the film thickness and binding energy dependence of the lifetimes of the hybridized QWS/IS states.

The very effect of the QWS/IS hybridization studied here for the thin metallic overlayers is essentially the same as has been observed for the rare gas adlayers at metal surfaces.[50,51,55–60] However, the overlayer thickness dependence of the many-body decay rates of the hybrid states is qualitatively different. The smooth increase of $\gamma^j_{e\text{-}e}$ with increasing overlayer thickness reported here has to be compared with the oscillating dependence found, e.g., for Xe/Ag(111), Kr/Cu(100), and Xe/Cu(100).[51,55] Such a qualitatively distinct results can be explained as due to the different electronic structure of metal and dielectric overlayers and different relaxation pathways of electronic excited states, as we discuss in the main text of the paper.

Finally, we would like to comment on the possibility of experimental verification of our findings. Predictions made in this paper can be tested in TR-2PPE experiments. Recent TR-2PPE measurements in Ref. 37 were reported up to the energies where QWS/IS hybridization takes place and its effect on the lifetime might be distinguished, according to our results. However, a conclusive comparison between present calculations and experiment requires larger Pb thickness range to be encompassed experimentally. The STS studies addressing the electronic states well above the Fermi level strongly perturb the system because of the tip-induced electric field.[61,74] ISs are transformed into the field emission resonances[75] characterized by a wave function pushed into the overlayer, which affects the decay rates.[76]

ACKNOWLEDGMENTS

Technical and human support provided by IZO-SGI, SGIker (UPV/EHU, MICINN, GV/EJ, ERDF, and ESF) is gratefully acknowledged. This work was partially funded by MCINN(FIS2010-19609-C02-01) and G.V-UPV/EHU(IT-366-07).

[1] S. Å. Lindgren and L. Walldén, Phys. Rev. Lett. **59**, 3003 (1987).
[2] T. Miller, A. Samsavar, G. E. Franklin, and T.-C. Chiang, Phys. Rev. Lett. **61**, 1404 (1988).
[3] M. Jałochowski, H. Knoppe, G. Lilienkamp, and E. Bauer, Phys. Rev. B **46**, 4693 (1992).
[4] C. Chiang, Surf. Sci. Rep. **39**, 181 (2000).

[5]Q. Qiu and N. V. Smith, J. Phys.: Condens. Matter **14**, R169 (2002).
[6]M. Milun, P. Pervan, and D. P. Woodruff, Rep. Prog. Phys. **65**, 99 (2002).
[7]S. Crampin, S. De Rossi, and F. Ciccacci, Phys. Rev. B **53**, 13817 (1996).
[8]J. J. Paggel, T. Miller, and T.-C. Chiang, Science **283**, 1709 (1999).
[9]L. Aballe, C. Rogero, P. Kratzer, S. Gokhale, and K. Horn, Phys. Rev. Lett. **87**, 156801 (2001).
[10]F. Schiller, A. Leonardo, E. V. Chulkov, P. M. Echenique, and J. E. Ortega, Phys. Rev. B **79**, 033410 (2009).
[11]A. Akjouj, L. Dobrzynski, and B. Djafari Rouhani, Phys. Rev. B **46**, 9808 (1992).
[12]P. M. Echenique and J. B. Pendry, J. Phys. C **11**, 2065 (1978).
[13]N. V. Smith, Phys. Rev. B **32**, 3549 (1985).
[14]A. L. Vázquez de Parga, J. J. Hinarejos, F. Calleja, J. Camarero, R. Otero, and R. Miranda, Surf. Sci. **603**, 1389 (2009).
[15]A. Ayuela, E. Ogando, and N. Zabala, Phys. Rev. B **75**, 153403 (2007).
[16]J. C. Boettger, Phys. Rev. B **53**, 13133 (1996).
[17]C. M. Wei and M. Y. Chou, Phys. Rev. B **66**, 233408 (2002).
[18]Y. Jia, B. Wu, H. H. Weitering, and Z. Zhang, Phys. Rev. B **74**, 035433 (2006).
[19]T. Miller, M. Y. Chou, and T.-C. Chiang, Phys. Rev. Lett. **102**, 236803 (2009).
[20]P. S. Kirchmann, M. Wolf, J. H. Dil, K. Horn, and U. Bovensiepen, Phys. Rev. B **76**, 075406 (2007).
[21]X. Ma, P. Jiang, Y. Qi, J. Jia, Y. Yang, W. Duan, W.-X. Li, X. Bao, S. B. Zhang, and Qi-Kun Xue, Proc. Natl. Acad. Sci. USA **104**, 9204 (2007).
[22]J. E. Ortega, F. J. Himpsel, G. J. Mankey, and R. F. Willis, Phys. Rev. B **47**, 1540 (1993).
[23]S. Yuasa, T. Nagahama, and Y. Suzuki, Science **297**, 234 (2002).
[24]U. Bauer, M. Dkabrowski, M. Przybylski, and J. Kirschner, Phys. Rev. B **84**, 144433 (2011).
[25]C. Koitzsch, C. Battaglia, F. Clerc, L. Despont, M. G. Garnier, and P. Aebi, Phys. Rev. Lett. **95**, 126401 (2005).
[26]A. G. Rybkin, A. M. Shikin, V. K. Adamchuk, D. Marchenko, C. Biswas, A. Varykhalov, and O. Rader, Phys. Rev. B **82**, 233403 (2010).
[27]H. Nienhaus, Surf. Sci. Rep. **45**, 1 (2002).
[28]P. Saalfrank, Chem. Rev. **106**, 4116 (2006).
[29]P. M. Echenique, R. Berndt, E. V. Chulkov, Th. Fauster, A. Goldmann, and U. Höfer, Surf. Sci. Rep. **52**, 219 (2004).
[30]E. V. Chulkov, A. G. Borisov, J. P. Gauyacq, D. Sánchez-Portal, V. M. Silkin, V. P. Zhukov, and P. M. Echenique, Chem. Rev. **106**, 4160 (2006).
[31]D.-A. Luh, T. Miller, J. J. Paggel, and T.-C. Chiang, Phys. Rev. Lett. **88**, 256802 (2002).
[32]Y.-F. Zhang, J.-F. Jia, T.-Z. Han, Z. Tang, Q.-T. Shen, Y. Guo, Z. Q. Qiu, and Q.-K. Xue, Phys. Rev. Lett. **95**, 096802 (2005).
[33]S. Mathias, M. Wiesenmayer, M. Aeschlimann, and M. Bauer, Phys. Rev. Lett. **97**, 236809 (2006).
[34]C. Brun, I. Po. Hong, F. Patthey, I. Y. Sklyadneva, R. Heid, P. M. Echenique, K. P. Bohnen, E. V. Chulkov, and W.-D. Schneider, Phys. Rev. Lett. **102**, 207002 (2009).
[35]I. Po. Hong, C. Brun, F. Patthey, I. Yu. Sklyadneva, X. Zubizarreta, R. Heid, V. M. Silkin, P. M. Echenique, K. P. Bohnen, E. V. Chulkov, and W-D. Schneider, Phys. Rev. B **80**, 081409 (2009).
[36]P. S. Kirchmann and U. Bovensiepen, Phys. Rev. B **78**, 035437 (2008).
[37]S. Mathias, A. Ruffing, F. Deicke, M. Wiesenmayer, M. Aeschlimann, and M. Bauer, Phys. Rev. B **81**, 155429 (2010).
[38]P. S. Kirchmann, L. Rettig, X. Zubizarreta, V. M. Silkin, E. V. Chulkov, and U. Bovensiepen, Nat. Phys. **6**, 782 (2010).
[39]L. Rettig, P. S. Kirchmann, and U. Bovensiepen, New J. Phys. **14**, 023047 (2012).
[40]D. Eom, S. Qin, M.-Y. Chou, and C. K. Shih, Phys. Rev. Lett. **96**, 027005 (2006).
[41]M. C. Yang, C. L. Lin, W. B. Su, S. P. Lin, S. M. Lu, H. Y. Lin, C. S. Chang, W. K. Hsu, and Tien T. Tsong, Phys. Rev. Lett. **102**, 196102 (2009).
[42]M. Becker and R. Berndt, Phys. Rev. B **81**, 205438 (2010).
[43]M. Becker and R. Berndt, Appl. Phys. Lett. **96**, 033112 (2010).
[44]S. M. Lu, W. B. Su, C. L. Lin, W. Y. Chan, H. L. Hsiao, C. S. Chang, and T. T. Tsong, J. Appl. Phys. **108**, 083707 (2010).
[45]A. Zugarramurdi, N. Zabala, V. M. Silkin, A. G. Borisov, and E. V. Chulkov, Phys. Rev. B **80**, 115425 (2009).
[46]X. Zubizarreta, V. M. Silkin, and E. V. Chulkov, Phys. Rev. B **84**, 115144 (2011).
[47]R. Fischer and T. Fauster, Phys. Rev. B **51**, 7112 (1995).
[48]K. Giesen, F. Hage, F. J. Himpsel, H. J. Riess, W. Steinmann, and N. V. Smith, Phys. Rev. B **35**, 975 (1987).
[49]D. Straub and F. J. Himpsel, Phys. Rev. Lett. **52**, 1922 (1984).
[50]X.-Y. Zhu, Surf. Sci. Rep. **56**, 1 (2004).
[51]J. Güdde and U. Höfer, Prog. Surf. Sci. **80**, 49 (2005).
[52]U. Höfer, I. L. Shumay, Ch. Reuß, U. Thomann, W. Wallauer, Th. Fauster, Science **277**, 1480 (1997).
[53]E. V. Chulkov, I. Sarría, V. M. Silkin, J. M. Pitarke, and P. M. Echenique, Phys. Rev. Lett. **80**, 4947 (1998).
[54]Th. Fauster, Ch. Reuß, I. L. Shumay, and M. Weinelt, Chemical Physics **251**, 111 (2000).
[55]J. D. McNeill, R. L. Lingle Jr., N.-H. Ge, C. M. Wong, R. E. Jordan, and C. B. Harris, Phys. Rev. Lett. **79**, 4645 (1997).
[56]C. M. Wong, J. D. McNeill, K. J. Gaffney, N.-H. Ge, A. D. Miller, S. H. Liu, and C. B. Harris, J. Phys. Chem. B **103**, 282 (1999).
[57]W. Berthold, F. Rebentrost, P. Feulner, and U. Höfer, Appl. Phys. A **78**, 131 (2004).
[58]A. Hotzel, G. Moos, K. Ishioka, M. Wolf, and G. Ertl, Appl. Phys. B: **68**, 615 (1999).
[59]K. J. Gaffney, C. M. Wong, S. H. Liu, A. D. Miller, J. D. McNeill, and C. B. Harris, Chemical Physics **251**, 99 (2000).
[60]M. Rohleder, W. Berthold, J. Güdde, and U. Höfer, Phys. Rev. Lett. **94**, 017401 (2005).
[61]A. Zugarramurdi, N. Zabala, A. G. Borisov, and E. V. Chulkov, Phys. Rev. B **84**, 115422 (2011).
[62]E. Ogando, N. Zabala, E. V. Chulkov, and M. J. Puska, Phys. Rev. B **71**, 205401 (2005).
[63]D. Yu and M. Scheffler, Phys. Rev. B **70**, 155417 (2004).
[64]K. Horn, B. Reihl, A. Zartner, D. E. Eastman, K. Hermann, and J. Noffke, Phys. Rev. B **30**, 1711 (1984).
[65]K. Jacobi, Phys. Rev. B **38**, 5869 (1988).
[66]E. V. Chulkov, V. M. Silkin, and P. M. Echenique, Surf. Sci. **391**, L1217 (1997); **437**, 330 (1999).
[67]A. Kiejna, Phys. Rev. B **47**, 7361 (1993).
[68]E. V. Chulkov, V. M. Silkin, and M. Machado, Surf. Sci. **482**, 693 (2001); **485**, 693 (2001)

[69]C. Leforestier, R. H. Bisseling, C. Cerjan, M. D. Feit, R. Friesner, A. Guldberg, A. Hammerich, G. Jolicard, W. Karrlein, H. D. Meyer, N. Lipkin, O. Roncero, and R. Kosloff, J. Comput. Phys. **94**, 59 (1991).
[70]D. Neuhauser and M. Baer, J. Chem. Phys. **91**, 4651 (1989)
[71]M. A. Van Hove, W. H. Weinberg, and C. M. Chan, *Low Energy Electron Diffraction* (Springer-Verlag, Berlin, 1986).
[72]E. G. McRae and M. L. Kane, Surf. Sci. **108**, 435 (1981).
[73]J. J. Quinn and R. A. Ferrell, Phys. Rev. **112**, 812 (1958).
[74]A. Zugarramurdi, N. Zabala, A. G. Borisov, and E. V. Chulkov, Phys. Rev. Lett. **106**, 249601 (2011).
[75]D. B. Dougherty, P. Maksymovych, J. Lee, M. Feng, H. Petek, and J. T. Yates Jr., Phys. Rev. B **76**, 125428 (2007).
[76]S. Crampin, Phys. Rev. Lett. **95**, 046801 (2005).